System-oriented Power Regulation Scheme for Wind Farms: The Quest for Uncertainty Management

Xue Lyu, *Member, IEEE*, Youwei Jia, *Member, IEEE*, Tao Liu, *Member, IEEE*, Songjian Chai, *Member, IEEE*

***Abstract*—High penetration of wind energy has intensified system pressure in balancing supply and demand due to the uncertainty nature of wind velocity. To mitigate the negative impacts brought along by wind power integration, an optimal power regulation scheme for a wind farm is proposed in this work. Specifically, the benefits of the designed wind power regulation scheme is innovatively quantified via the reduction of balancing cost. To handle wind uncertainty while determining generation profile for the wind farm, a robust strategy is introduced in the proposed control. In addition, the aerodynamic interactions among wind turbines are considered. To bypass the nonlinearity and non-convexity involved in the optimization problem and achieve online application, an artificial intelligence aided control is newly designed. Simulation results demonstrate the good performance of the proposed control scheme under multiple operation scenarios.**

***Index Terms*—Wind farm, wind power regulation, optimal control, online application**

NOMENCLATURE

P_m	Mechanical power capture by a WT
ρ	Air density
R	WT rotor radius
v_w	Wind speed
C_p	Power coefficient
β	WT Pitch angle
λ	WT Tip speed ratio
ω_r	WT rotor speed
P_{ref}^{mppt}	Active power reference generated from MPPT algorithm
P_{wtnom}	Nominal power of a WT
J	WT equivalent moment inertia
T_m	WT aerodynamic torque
T_e	WT electrical torque
η	WT gear box ratio
δv_w	Aggregated velocity deficit of a WT
C_T	WT thrust coefficient
k	Decay constant
$\gamma_m(k)$	Mileage payment of an AGC unit m at time slot k
$D_m(k)$	Regulation mileage of unit m at time slot k
S	Mileage price
K_m	Performance score of unit m
P_{ke}	Electric power converted from kinetic energy charging/discharging process
P_e	Electric power output of a WT
Δt	Control interval
α	Weighting factor in the multi-objective optimization
P_{wfnom}	Nominal power of the WF
$\omega_{ropt}(\beta)$	Rotor speed that ensures the maximum power capture under a certain β
$P_{load}(k)$	Load demand at time slot k
$P_{schedule}(k)$	Scheduled power at time slot k
$D_m^{up}(k)$	Up regulation mileage of unit m at time slot k
$D_m^{down}(k)$	Down regulation mileage of unit m at time slot k
$P_m^{reg\_up}(k)$	Up AGC set points of unit m
$P_m^{reg\_down}(k)$	Down AGC set points of unit m
P_{reg_cap}	Regulation capability of an AGC unit
$\hat{\mathbf{q}}^{\tau}$	Sequence of predicted quantiles
l	Loss function
τ	Target quantile
y_{k+i}	Observation at time slot $k+i$

This work was supported in part by Natural Science Foundation of China (72071100), Guangdong Basic and Applied Basic Research Fund (2019A1515111173), Dept. of Education of Guangdong Province under Young Talent Program (2018KQNCX223), the RGC of the Hong Kong Special Administrative Region under the General Research Fund (17209219) and the Joint Research Fund in Smart Grid (U1966601) under cooperative agreement between the National Natural Science Foundation of China (NSFC) and State Grid Corporation of China (SGCC). (*Corresponding author: Youwei Jia*)

X. Lyu is with the Department of Electrical and Electronic Engineering, Southern University of Science and Technology, Shenzhen, China, and is also with the Department of Electrical and Electronic Engineering, The University of Hong Kong, Hong Kong. (e-mail: xuelu111@gmail.com)

Y. Jia is with the Department of Electrical and Electronic Engineering, Southern University of Science and Technology, Shenzhen, China. (e-mail: jiayw@sustech.edu.cn)

T. Liu is with the Department of Electrical and Electronic Engineering, The University of Hong Kong, Hong Kong. (e-mail: taoliu@eee.hku.hk)

S. Chai is with the College of Physics and Optoelectronic Engineering, Shenzhen University, Shenzhen. (e-mail: chaisongjian@gmail.com)

$\hat{q}_{k+i}^{\tau}$	Predicted quantile at time slot $k+i$
$\mathcal{D}(x,y)$	Training dataset
$\bar{b}(x_n)$	Ensemble collective output of an individual learner
e_i	De-correlated error of an individual learner
w_i	Weight of the i-th based network
b_{i}	Output of the i-th based network
σ	Regularizing factor
$b_i(x_n)$	Output of the i-th based network
χ_{ij}	Output weight of the j-th hidden neuron in the i-th base model
$g_{ij}(x_n)$	Output of j-th hidden neuron in the i-th base model
ΔP_{comp}	Compensated power
$\Delta\beta_{comp}$	Compensated pitch angle
$P_m^{opt(\beta)}$	Mechanical power captured by a WT at $\omega_{ropt}(\beta)$
P_{com}	Active power command of a WT
β_{com}	Pitch angle command of a WT
P_{meas}	Measured actual output power from a WT

I. Introduction

THE worldwide installation capacity of wind power has grown rapidly in recent years. However, the wind power generation is highly dependent on external environment (i.e., wind speed), which is difficult to predict accurately. To yield the maximum power production, wind turbines (WTs) usually operate at the maximum power point tracking (MPPT) mode. This control strategy intensifies the fluctuation nature of wind power, which in turn leads to the phenomenon that system operators would require more fast reserve to counterbalance the imbalance between generation and demand [1].

The instantaneous power balance between supply and demand should be maintained to guarantee power system stable operation. The concept of "regulation mileage" is firstly put forward by PJM and then soon widely accepted by several independent system operators (e.g. CAISO, NYISO, ISO-NE, MISO and China Southern Power Grid (CSG)) to encourage the fast-responding generators to participate in the regulation market. In a performance-based balancing market, the regulation mileage can be regarded as essential regulation "products" and should be traded periodically. That is, under such ancillary service environment, AGC units can earn profits by assisting in power balance. Correspondingly, utilities pay for such regulation service that is counted as mileage payment. With increasing penetration of wind power, the balancing cost incurred by wind power fluctuations would be very high [2]. As reported in [3], the balancing costs due to wind variability and uncertainty amounts to about 1-4.5€/MWh when the wind penetration reaches up to 20%. To address this issue, some market policies have been made to force the owner of wind farms (WFs) to share the balancing costs. For example, the WF owner is required to pay a fixed balancing fee per MWh or MW-month [4]. According to [5], a fine would be imposed if the actual wind power production deviates from the day-ahead forecasted. However, it is difficult to precisely quantify to which extent the incurred balancing cost should be shared by the WF in real-time operation. Besides, wind turbine generators can hardly be dispatched like conventional generators due to the stochastic nature of wind. This prompts a discussion on how to design a proper control strategy for WFs to enable them to be balancing responsible.

Smoothing wind power fluctuations is a feasible solution to reduce balancing cost. In some pioneering works [6-9], the hard-coded algorithms (e.g., low pass filter, moving average filter, and power ramp limits) are utilized to generate smoothing references. However, the references generated via these methods are decoupled from system balancing needs. A preliminarily work along this direction is reported in our previous work [10], where a system perceived optimization technique is used to generate the smooth reference. Whereas the wind uncertainty and aerodynamic interactions amongst WTs are not considered. It should be noted that wind farms face more pressure when participating in the balancing market due to the uncertainty nature of wind speed. Furthermore, the aerodynamic coupling among WTs exacerbates the complexity of wind power regulation. Considering the nonlinearity and non-convexity of the WT model and wake model [11] (i.e. there is a wake behand a rotor, which expands and diminishes with distance), achieving online optimal wind power regulation is an essential yet challenging issue.

Recently, several system operators require WFs to communicate with the dispatch center. For example, in Spanish market [12], a WF with rated capacity being larger than 10 MW is requested to connect to a delegate dispatch center. In this connection, this paper explores to develop an optimal power regulation scheme for a WF to mitigate the negative impact brought along by wind power fluctuations. The main contributions of this paper are threefold:

i) The overall power output from the WF can be optimally regulated via properly exploiting the downward and upward power regulation capabilities of WTs.

ii) The wind prediction accuracy is considered and a robust strategy is developed to handle wind power uncertainty when determining the generation profile of the WF.

iii) The detailed WT model and wake model are comprehensively considered in the proposed control scheme. Moreover, the proposed control can be online implemented via introducing an artificial intelligence (AI) aided method.

II. Related Studies and Proposed Methodology

To manage wind power uncertainty, an effective method is to combine WFs with some other resources to form a virtual power plant [13-16]. For example, a combined heat and power (CHP) plant and WF system is modeled and operated as a portfolio in [13] to decrease the total net imbalance. The power-to-gas (P2G) facilities and WFs are coordinated in [14] to maximize the joint profit. A profit-sharing mechanism for the concentrating solar power (CSP) and WFs is developed in [15]. In these reported works, WFs are assumed to purchase reserve from the other flexible resources to avoid high imbalance

penalties. Instead of relying on additional resources, the WF in [16] commits some of its own reserve to offset the negative impact of wind power uncertainty. Also, a security constrained optimal consensus distributed control strategy is proposed in [17] to effectively promote the integration of surging wind power.

It should be noted that the abovementioned works focus on determining the day-ahead offers for the WF which has a relatively long cycle of energy scheduling. Moreover, the detailed WTs model and their operating characteristic are not considered. Distinguished from these existing works, this work aims to develop an optimal power regulation scheme for a WF in the real-time regulation market, where the practical constraints of WTs are taken into account.

At the WF level, the main issue is to regulate the aggregated power generation. The wake effect among WTs may cause a significant power production reduction and adds extra difficulties to achieve optimal control. According to [18], the total wind power losses due to wake effects is considerable (i.e. the wind power loss can reach up to 23% at the worst case). To mitigate the negative impact of wake effect and maximize overall power production from WFs, different optimization techniques are adopted including the heuristic methods (e.g. particle swarm optimization (PSO) and genetic algorithm (GA) [19, 20]) and data-driven methods (e.g., Bayesian ascent, game-theoretic search [21, 22]). Except for pursing wind power maximization, optimization objectives such as kinetic energy (KE) maximization, KE maximization while keeping a certain amount of de-loading capacity are investigated in [23, 24]. However, it is usually time-consuming to derive an optimal solution due to the nonlinearity and non-convexity of the formulated optimization problems. As a consequence, these methods cannot be applied to online application. At the WT level, the main issue is to follow the dispatch command via its self-regulation capability. Control methods developed in this research filed can be divided into two main categories: the rotor speed regulation based control and pitch angle regulation based control.

To tackle abovementioned problems, a novel control scheme for a WF is designed in this work. Fig. 1 gives an overview of the proposed control scheme. At the optimization layer, a receding horizon optimization method is utilized to determine the generation profile of the WF. Specifically, to deal with the worst scenario, the interval forecasting technique is used and the most fluctuated case in the look-ahead time window is chosen for receding horizon optimization. The update cycle of the WTs dispatch commands is identical with the AGC cycle. To facilitate online optimization, a de-correlated neural network ensembles (DNNE) algorithm is introduced. At WTs control layer, the rotor speed regulation based control and pitch angle regulation based control are utilized simultaneously to trace the periodic dispatch commands. The proposed control scheme has threefold advantages: 1) the dispatch commands for WTs is generated from a system-oriented perspective; 2) the negative impact of wind uncertainty is handled by a robust strategy; 3) high computational efficiency is guaranteed with a simple matrix calculation.

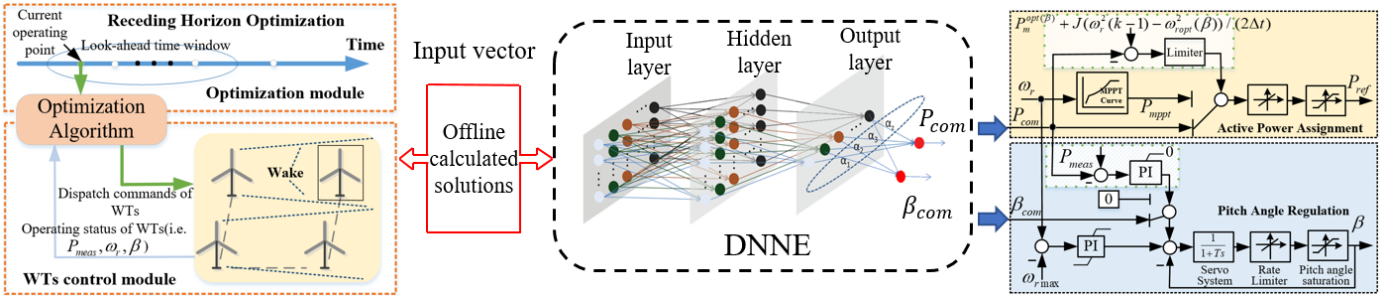

Fig. 1. Framework of the proposed control scheme

III. Wind Turbine and Wake Effect Models

A. Wind Turbine Model

The mechanical power that a WT extracts from wind is

$$P_m = \frac{\rho}{2}\pi R^2 C_p(\lambda,\beta)v_w^3 \tag{1}$$

where ρ is the air density; R is the rotor blade radius; v_w is the wind speed, β is the pitch angle, C_p is the power coefficient; and λ is the tip speed ratio defined as

$$\lambda = \frac{\omega_r R}{v_w} \tag{2}$$

with ω_r being the rotor speed.

To get the maximum power, the pitch angle needs to be maintained at zero degree while the rotor speed should vary according to wind speed when the wind speed is below the rated value; on the other hand, the rotor speed should maintain at its rated value while the pitch angle control starts to activate when the wind speed is higher than the rated value. The active power reference of a WT under the MPPT control (P_{ref}^{mppt}) can be expressed as,

$$P_{ref}^{mppt} = \begin{cases} \frac{\rho}{2}\pi R^2 C_p(\lambda_{opt,\beta=0},0)v_w^3, & v_w \le v_{wrated} \\ P_{wtnom}, & v_w > v_{wrated} \end{cases} \tag{3}$$

where P_{wtnom} denotes the WT's nominal power (i.e. the captured power at the rated wind speed), v_{wrated} is the rated wind speed.

This work considers the doubly-fed induction generator (DFIG) based WT. We assume that the drive train is rigidly coupled, and the single mass model is adopted

$$J\frac{d\omega_r}{dt} = T_m - \eta T_e \tag{4}$$

where J denotes the equivalent moment inertia of the WT; η denotes the gear box ratio; $T_m = P_m / \omega_r$ is the aerodynamic

torque; and $T_e = P_e / (\eta \omega_r)$ is the electrical torque.

B. Wake Effect Model

WTs extract energy from wind and there is a wake effect behind the turbine, i.e. the wind speed reaching to downstream WTs is less than that of upstream WTs. Various wake effect models have been proposed in the literature. Among these models, the Jensen's wake effect model is the most prevalent one and is suitable for engineering applications. It is established based on the assumption that the wake effect expands linearly downstream, as shown in Fig. 2. For any WT $j \in B$ with B being the total number of WTs in the WF, the velocity profile can be given by,

$$v_{wj} = v_{w0}(1 - \delta v_{wj}) \tag{5}$$

where v_{w0} is the free wind speed, δv_{wj} is the aggregated velocity deficit of WT j. Taking the multiple wakes generated by upstream WTs into account, δv_{wj} can be expressed as

$$\delta v_{wj} = \sum_{j \in N: x_i < x_j} (1 - \sqrt{1 - C_{Ti}})\left(\frac{D_j}{D_i + 2dx_{j \to i}}\right)^2 \frac{\mathrm{A}_{i \to j}^{shadow}}{A_j} \tag{6}$$

Here, D_i is the diameter of the blades of the i-th WT. C_{Ti} is the thrust coefficient and is a nonlinear function of the tip speed ratio and pitch angle. $x_{j \to i}$ is the distance between the upstream WT i and downstream WT j along with the wind direction. $\mathrm{A}_{i \to j}^{shadow}$ is the overlap between the area spanned by the wake shadow cone generated by WT i and the area swept by the WT j (i.e. A_j). d is the decay constant.

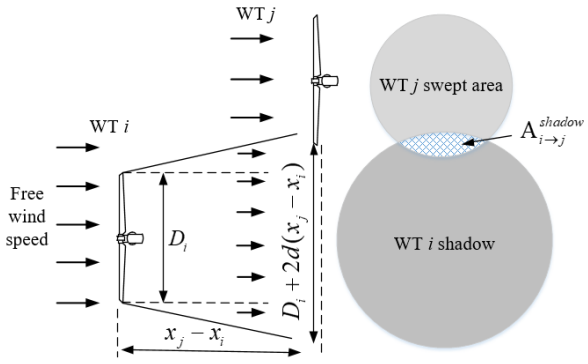

Fig. 2. Jensen's wake model

IV. The Proposed System-oriented Power Regulation Scheme for a Wind Farm

A. Mileage Payment Estimation

The mileage payment reflects the speed and accuracy that a regulation resource in following the Automatic Generation Control (AGC) signal. At a certain time slot k, the mileage payment system operator compensates to an AGC unit m can be calculated as a product of three terms,

$$\gamma_m(k) = | D_m(k) | \cdot S \cdot K_m \tag{7}$$

In (7), $D_m(k)$ is the regulation mileage (i.e. the up/down movement of the m-th AGC unit to follow AGC dispatch signal) at time slot k; S is the mileage price which is market-dependent; K_m is the performance score which evaluates the performance of the m-th unit in terms of following the AGC dispatch signal and it can be calculated once for each market interval.

Originally, a significant part of mileage payment would be caused by the randomness of wind energy. Even though wind turbine generators can hardly be dispatched like conventional generators. To a considerable extent, regulating wind power actively in response to actual system needs would have a positive impact on mitigating system balancing pressure. In this connection, it would be much interesting and reasonable to regulate wind power by considering a WF as a semi-dispatch resource other than passive "free-runners". Hence in this work, we hold a perspective that the WF should be balancing responsible.

The "benefited pay" principle is an ideal rule in the balancing market. However, this impartial principle is fairly difficult to achieve, as it is difficult to precisely quantify to which extent the incurred balancing cost should be shared by the beneficiaries in real-time operation. As recalled our initial incentive—by letting the WF be balancing responsible, the mileage payment should be somehow pre-estimated and such mileage payment can be regarded as an important indictor to regulate wind power generation. Such operation strategy coincides with the above-mentioned "benefited pay" principle and fits in with an efficient and fair market environment.

As illustrated above, the wind farm output should be timely controlled and respond to the real-time mileage payment. Based on this, we include AGC information as an essential part to pre-estimate the AGC actions, which should be consistent with the actual ones. In context of the concerned market structure and operation mechanism in this paper, the information of AGC units covering energy scheduling profile, regulation capability, performance score, etc. should be available for system operators. In this connection, the mileage payment can be pre-estimated from the WF perspective.

B. Principle of Wind Power Regulation

Fig. 3 gives the power capture characteristic of a WT. Initially, suppose a WT operates at point A according to the MPPT algorithm at a certain wind speed. If less wind power output is expected, the WT can choose to shift to point B or C by accelerating rotor speed or increasing pitch angle. If the former method is adopted, a part of excessive energy can be stored in the rotational rotor. If more wind power is expected in the near future, the WT can shift to point D via rotor speed deceleration as the stored KE can be released back to system. If the latter method is adopted, the overloading would not be achieved. In WTs real-time operation, we can regulate the power outputs of WTs via utilizing rotor speed regulation based control or blade pitch angle regulation based control.

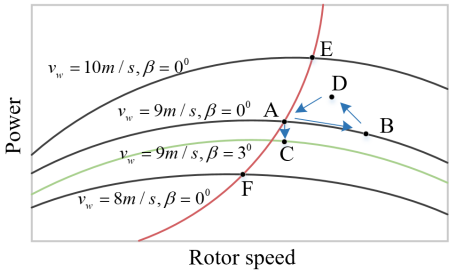

Fig. 3. Power capture characteristic of a WT

1) Rotor Speed Regulation based Control

For a WT, when it works at a de-loading mode, the excessive wind energy can be stored in the rotating mass via rotor speed acceleration till the upper limit is reached. Similarly, the KE stored in the rotating mass can be released back to system via rotor speed deceleration. In particular, the KE stored in its rotating mass is

$$E = \frac{1}{2} J \omega_r^2 \tag{8}$$

and the electric power converted from KE charging/discharging process (i.e. P_{ke}) can be formulated as,

$$P_{ke} = \frac{dE}{dt} = J \omega_r \frac{d\omega_r}{dt} \tag{9}$$

It should be noted there exists a rotor speed denoted as $\omega_{ropt}(\beta)$ that captures the maximum power under a certain pitch angle (e.g. point A, E, F in Fig. 3). If the rotor speed decelerates to a value that lower than $\omega_{ropt}(\beta)$, the WT would require extra power to bring the rotor speed to recover to $\omega_{ropt}(\beta)$. As a consequence, during this process, the active power dip would occur. Besides, according to [25], operating at a status that the rotor speed is lower than $\omega_{ropt}(\beta)$ may reduce system small signal stability margin. Therefore, the rotor speed variation limits should be considered when adopting the rotor speed regulation based control.

2) Pitch Angle Regulation based Control

Different from the rotor speed regulation based control, overloading cannot be achieved via the pitch angle regulation based control as no energy storage component exists in the pitch angle controller. Instead, the mechanical power captured by the WT is directly changed via pitch angle variation.

At the WT level, the rotor speed regulation based control is usually preferable due to the high energy efficiency and fast response. However, at the WF level, utilizing the rotor speed regulation based control and pitch angle regulation based in a cascaded manner is no longer the optimal solution due to wake effect. As illustrated in (5), (6), the wind speed at downstream WTs is influenced by the operating status of upstream WTs, which in turn influences the overall power production of the WF. To optimally exploiting the overall power regulation capability of the WF, an optimization problem would be formulated in the next section.

C. The Optimization Module

1) Problem Formulation

According to the above-mentioned analyse, the imbalance between the scheduled power and net load can be mitigated by regulating wind power output. Therefore, for the WF operator, wind power maximization should not be the only target and the balancing cost incurred by wind power fluctuation should be taken into account at the same time. These two competing objectives (i.e. wind power maximization and mileage payment minimization) are achieved via multi-objective optimization in this work.

According to (1) and (9), the electric power that an individual WT delivers to the grid is

$$P_e(t) = P_m(t) - P_{ke}(t) \tag{10}$$

Discretizing the above equation, gives

$$P_e(k) = \frac{1}{2} \rho \pi R^2 C_P(\lambda(k), \beta(k)) v_w^{\,3}(k) - J \omega_r(k) \frac{\omega_r(k) - \omega_r(k-1)}{\Delta t} \tag{11}$$

where Δt is the length between two consecutive time instants k and k-1. In this work, the wind speed is assumed to be constant for the short control interval Δt.

According to (11), the power output from a WT at current time slot k is dependent on the operation status at time slot k-1. To achieve optimal wind power regulation, a receding horizon optimization technique is adopted in this work. In the receding horizon optimization, the dispatch decision of the first control cycle is executed and then the process is repeated from the new current state for future decision making. In a given look-ahead time window (i.e. from current time slot k_0 to future time slot k_H), the optimization problem is formulated as follows,

$$\max_{\omega_{rb},\, \beta_b} \ \alpha \sum_{k_0}^{k_H} \sum_{b=1}^{B} P_{eb}(k) \Delta t / P_{wfnom} - (1-\alpha) \sum_{k_0}^{k_H} \sum_{m=1}^{M} (D_m^{up}(k) + D_m^{down}(k)) S K_m / C_{mil\max} \tag{12}$$

s.t.

$$0 \le P_{eb}(k) \le 1.2 P_{wtnom} \tag{13}$$

$$\omega_{roptb}(\beta_b)(k) \le \omega_{rb}(k) \le \omega_{r\max} \tag{14}$$

$$\beta_{\min} \le \beta_b(k) \le \beta_{\max} \tag{15}$$

$$D_m^{up}(k) = P_m^{reg\_up}(k) - P_m^{reg\_up}(k-1) \tag{16}$$

$$D_m^{down}(k) = P_m^{reg\_down}(k-1) - P_m^{reg\_down}(k) \tag{17}$$

$$0 \le P_m^{reg\_up}(k) \le P_m^{reg\_cap} \tag{18}$$

$$0 \le P_m^{reg\_down}(k) \le P_m^{reg\_cap} \tag{19}$$

$$P_{load}(k) - \sum_{b=1}^{B} P_{eb}(k) = P_{schedule}(k) + \sum_{m=1}^{M} (D_m^{up}(k) - D_m^{down}(k)) \tag{20}$$

var $\omega_{rb}(k),\ \beta_b(k) \in \mathrm{R}^+,\ k \in [k_0, k_T], b \in [1, B]$

In the objective function, B is the number of WTs, M is the number of AGC units and α, S, K_m are defined in (7), P_{wfnom} denotes the WF nominal power and $C_{mil\max}$ denotes the maximum mileage payment. The weighting factor $\alpha \in [0,1]$ can be used to achieve a balance of the trade-off between the two objectives. Specifically, decreasing α can stimulate the WF to release system balancing stress whereas the harvested wind energy would be decreased in the meantime. Even though the decrease of wind energy harvesting is inevitably unavoidable after the WF being balancing responsible. However, instead of arbitrarily sacrificing a significant amount of wind energy, our proposed strategy can response to the estimated system balancing needs subject to the practical constraints of the wind turbines.

WTs constraints: Physical constraints of WTs such as the available power, rotor speed and pitch angle are considered. In particular, the maximum active power injection from a WT is determined by the converter limit, which further depends on the

maximum value of the converter voltage and the maximum current rating. Such a setting can be adjusted according to the characteristic of power electronic devices. For example, in [26], the maximum value of the converter active power injection is 1.21 p.u. when the design power factor of the converter equals to 1; In [27], the converter limit is assumed to be 1.2 p.u.. In this work, we assume that the converter limit is 1.2 p.u., as shown in (13). To guarantee the stable operation of WTs, the rotor speed variation is limited via (14). The pitch angle variation should be within WTs physical limits, as shown in (15), where $\omega_{ropt}(\beta)$ is obtained using a look-up table method.. It is noted that wake interactions are modeled in the optimization formula and wind speeds experienced by down-WTs are calculated according to (5) and (6).

System constraints: $D_m^{up}(k)$ / $D_m^{down}(k)$, $P_m^{reg\_up}(k)$ / $P_m^{reg\_down}(k)$ denotes the up/down regulation mileage, up/down set points of AGC unit m at time slot k respectively, $P_m^{reg\_cap}$ denotes the regulation capability of AGC units m. The AGC units that participate in the regulation market should subject to their operational constraints. As given in (18), (19), the AGC set points should be limited by the regulation capabilities of each unit. Besides, in real time operation, the system should subject to the power balancing constraint (20).

2) Wind Forecasting in the Receding Horizon

In this work, the traditional point forecasting method is not used as this method is hardly to be accurate enough. Instead, the well-known long short-term memory (LSTM) network [28] is adopted to construct wind speed prediction intervals (PIs) over multiple look-ahead horizons. The LSTM network is a powerful tool for general-purpose sequence modeling, which is essentially a variant of recurrent neural network (RNN). In this work, the encoder-decoder (Seq2Seq) LSTM architecture is adopted to generate a bunch of desired quantiles, and then the PIs are derived based on several pairs of the estimated quantiles. For instance, quantiles with levels of 5% and 95% form a 90% PI. In this sense, the underlying problem can be formulated as a quantile regression problem,

$$\hat{\mathbf{q}}^{\tau} = f(\tilde{x}_k; \boldsymbol{\theta}) \tag{21}$$

where $\hat{\mathbf{q}}^{\tau} = \left\{\hat{\mathbf{q}}^{\tau}_{k+1}, \ldots \hat{\mathbf{q}}^{\tau}_{k+H}\right\}$ is the H-step sequence of predicted quantiles with different levels ranging from τ_1 to τ_Q, $\tau \in [0,1]$, $\tilde{x}_k$ is the explanatory information available up to time k, $\boldsymbol{\theta}$ is the parameters of estimator $f(\cdot)$ which needs to be tuned. As shown in Fig. 4, the encoder is composed of several stacked LSTM units, each accepts the current input x_k and the outputs (cell and hidden states) from the previous unit. It propagates forward until the last unit of encoder generates the decoded features, which also acts as the input for the first unit of decoder. The cell and hidden states also propagate forward until the ending of forecasting horizon. Finally, the forecasted sequence is obtained.

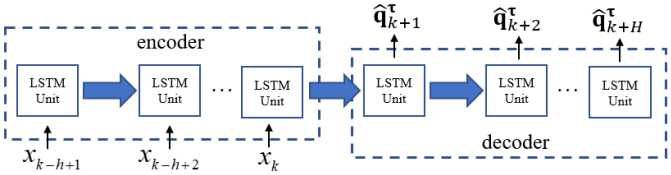

Fig. 4. LSTM encoder-decoder model

The accuracy of predicted quantiles is evaluated through the popular statistical metric---pinball loss [29], herein the asymmetric weights are applied to errors through a tilted transformation of the absolute value function as follows,

$$l^{\tau}(y_{k+i}, \hat{q}^{\tau}_{k+i}) = \begin{cases} \tau(y_{k+i} - \hat{q}^{\tau}_{k+i}), & if\ y_{k+i} \geq \hat{q}^{\tau}_{k+i} \\ (1-\tau)(\hat{q}^{\tau}_{k+i} - y_{k+i}), & if\ y_{k+i} < \hat{q}^{\tau}_{k+i} \end{cases} \tag{22}$$

where y_{k+i} is the observation at time slot $k+i$. The lower pinball loss value indicates a better predictive performance of the model. As a result, the learning process of encoder-decoder LSTM translates to an optimization problem defined by,

$$\arg\min_{\theta} \sum_{k=1}^{T} \sum_{\tau_1}^{\tau_Q} \sum_{i=1}^{H} l^{\tau}(y_{k+i}, f(x_{k-h+1}, \cdots x_k; \theta)) \tag{23}$$

where is T is the number of trained time slots.

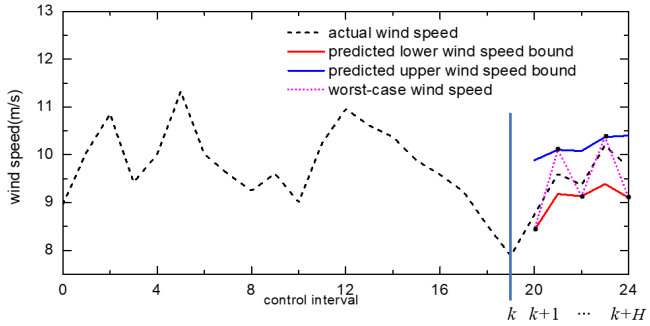

Fig. 5. The robust strategy for the receding horizon optimization

To cope with wind power uncertainty, a robust strategy is introduced for wind power regulation by deploying the resultant forecasting interval. Under a certain PI, for time window [k+1, k+H], the actual wind speed, and the predicted upper/lower prediction bounds are given in Fig. 5. To mitigate system balancing pressure, the most fluctuated wind speed in the concerned time window (the dot pink line in Fig. 5) is selected as input information for the receding horizon optimization. As a result, the mileage payment can be minimized even under the worst case.

Remark: The more volatile the wind speed is, the more mileage cost would be incurred.

3) Online Application of the Proposed Control

Owing to the nonlinearity and non-convexity of the abovementioned optimization problem, the analytical optimization techniques is no longer applicable and the PSO algorithm is utilized to solve the problem. It should be noted this method cannot be directly applied to online control as it needs a relatively long computing time.

The artificial neural networks (ANNs) can be regarded as a black-box to map the given input to the desired output via learning from data and finding a hypothesis to estimate the unknown target function. In recent years, they are widely used for classification, prediction, and function approximation. To enable the proposed scheme can achieve online application, an

intelligent learning based method is introduced in this work. It is noted that the incentive of proposing the intelligent learning based predictor is to facilitate online optimization. Owing to its unique merit (i.e. fast training mechanism), it can serve as a promising alternative solution method.

Considering the complex nonlinear relationship between the input variables and output variables in the formulated problem, an ensemble learning approach is utilized in this work. Specifically, the random vector functional-link (RVFL) networks are selected as ensemble component models to overcome the disadvantages of the gradient-based learning algorithms for training the single-layer feed-forward networks (e.g. local minima, slow convergence, poor sensitivity to learning rate setting). To encourage the diversity among ensemble components and meanwhile maintain an overall good ensemble accuracy, a de-correlated neural-net ensembles method is utilized in this work. The network architecture of the DNNE model is given in Fig. 1. Given an ensemble of z base model and a training dataset $\mathcal{D}(x,y)$ containing s instances, the ensemble collective output and the de-correlated error of i-th individual learner are formulated as,

$$\bar{b}(x_n) = \sum_{i=1}^{z} w_i b_i(x_n) \tag{24}$$

$$e_i = \sum_{n=1}^{s} [\frac{1}{2}(b_i(x_n) - y_n)^2 - \sigma(b_i(x_n) - \bar{b}(x_n))^2] \tag{25}$$

where w_i , b_i are the weight and the output of the i-th base network respectively, $\sigma \in [0,1]$ is a regularizing factor.

To attain a reliable and accurate ensemble output, the weight of each base learner (i.e. w_i) is determined by the learning performance of each RVFL net. In particular, an entropy based weights selection method is utilized to quantify the performance of each RVEL net, and the details can be referred to [30].

For an individual learner, the output of the i-th base network (simulated with an instance x_n) can be expressed as,

$$b_i(x_n) = \sum_{j=1}^{L} \chi_{ij} g_{ij}(x_n) \tag{26}$$

where L is the number of hidden neurons in the i-th individual RVFL network; χ_{ij} is the output weight of the j-th hidden neuron in the i-th base model; $g_{ij}(x_n)$ is the output of j-th hidden neuron in the i-th base model and $g(\cdot)$ can be any squashing basis function.

It is assumed that all base learners have homogeneous hidden nodes. Hence the negative correlation learning ensemble models would obtain the optimal performance when the gradient of error expressed in (26) vanishes. The detailed matrix calculation process can be referred to [30].

In the proposed problem, the wind speed prediction data in the look-ahead time window, rotor speed and pitch angle of WTs at previous time slot, the mileage price, scheduled power, load demand and performance score of AGC units in the look-ahead time window constitute the input vector. The optimal dispatch commands of individual WTs (i.e. active power command and blade pitch angle command) are the target vector.

D. Wind Turbines Control Module

The rotating mass builds up an "energy buffer" such that the wind power production can be extended via KE charging/discharging. In addition, the mechanical power capture efficiency of the WT can be directly changed via pitch angle regulation. The rotor speed regulation based control and pitch angle regulation based control work simultaneously in this paper to adjust wind power output. As shown in Fig. 1, that the original MPPT control is bypassed and the active power command and pitch angle command of individual WTs that generated from the optimization module are sent to WTs' rotor side converter and pitch controller as the new reference set-points. In real-time operation, to guarantee the stable operation of WTs and to ensure that the predicted active power command and the pitch angle command matching up with the operating principle of WTs, two refining loops are introduced into WTs' control module.

As mentioned in Section IV. B, the rotor speed over-deceleration during KE discharging process should be avoided. To this end, an active power compensation loop is designed and the compensate value of the power command ΔP_{comp} can be expressed as,

$$\Delta P_{comp} = \min\left\{P_m^{opt(\beta)} + \frac{J(\omega_r^2(k-1) - \omega_{ropt}^2(\beta))}{2\Delta t} - P_{com}, 0\right\} \tag{27}$$

where $P_m^{opt(\beta)}$ is the optimal mechanical power that the WT captures at $\omega_{ropt}(\beta)$, $\omega_r(k-1)$ is the rotor speed at previous time slot. After introducing (27), the power command would never larger than $P_m^{opt(\beta)} + \frac{J(\omega_r^2(k-1) - \omega_{ropt}^2(\beta))}{2\Delta t}$, which in turn guarantees the stable operation of the WT.

A pitch angle compensation loop is also developed to avoid the over adjustment of blade pitch angle. As given in Fig. 1, the mismatch between the measured actual wind power output and the active power command is sent to a Proportion-Integration controller, and then a compensation value of the pitch angle command is generated to eliminate the deviation between the actual power output and the dispatch command. After adding this loop, the pitch angle reference can be refined, and the compensate value of the pitch angle command $\Delta\beta_{comp}$ can be expressed as,

$$\Delta\beta_{comp} = \min\left\{K_p(P_{com} - P_{meas}) + K_I\int(P_{com} - P_{meas}), 0\right\} \tag{28}$$

where K_P and K_I are the control parameters of the Proportion-Integration controller.

V. Case Studies

A. Experimental Setup

In this section, we test our method in a modified IEEE 9-bus test system, in which a 100 MW-WF is integrated. As shown in Fig. 6, the WF has 20 units of WTs. Specifically, there are five rows and each row consists of four WTs in the WF, where the space of two adjacent DFIGs is 5D. For WTs in the WF, the NREL 5 MW DFIG-WT is utilized and the detailed parameter

setting can be found in [31]. More information about the test system can be found in [32].

In this work, the system dynamic model is developed in DIgSILENT/PowerFactory, and the optimization framework is formulated in MATLAB. The set-up of the joint simulation platform guarantees the bidirectional data exchange. Specifically, the AGC control cycle is set to 4 seconds. The look-ahead time window in the optimization module is set as 5 times of the AGC cycle (i.e. 20 s). The simulation was executed on a computer of 2 processors, each one with 2.59 GHz frequency, and 64 GB of RAM.

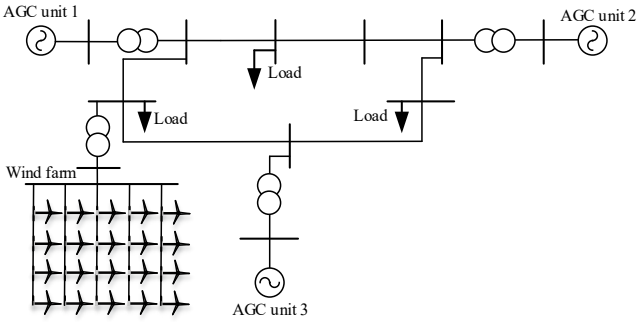

Fig. 6. Testing system configuration

In this work, the system dynamic model is developed in DIgSILENT/PowerFactory, and the optimization framework is formulated in MATLAB. The set-up of the joint simulation platform guarantees the bidirectional data exchange. Specifically, the AGC control cycle is set to 4 seconds. The look-ahead time window in the optimization module is set as 5 times of the AGC cycle (i.e. 20 s). The simulation was executed on a computer of 2 processors, each one with 2.59 GHz frequency, and 64 GB of RAM.

B. Simulation Results and Analysis

1) Performance of the Trained DNNE

It takes about 17 min on average to find a solution of the optimization problem using PSO algorithm. Obviously, it cannot be directly applied to online control. The offline calculated solutions are collected to train DNNE. In fact, one cannot exhaustively simulation every possible scenario offline. Regarding this concern, we would like to firstly justify the validity of the selective training set. In our case studies, a total of 8097 samples covering typical operation states are obtained by offline calculation by using the particle swarm optimization (PSO) algorithm, among which 7000 of them are adopted to train DNNE and 1097 of them are used to test the proposed control scheme. The wind speed data for offline calculation is captured from [33]. The mean absolute percentage error (MAPE) and normalized root-mean-square error (nRMSE) are used to evaluate the performance. The detailed results are given in Table I, which demonstrates that the prediction accuracy the DNNE algorithm is satisfactory. It should be noted that in real-world application, it is indeed possible to further extend the training set and re-tune the whole DNNE model to enhance the optimization process in considering other unseen operation states.

TABLE I
TABLE I PREDICTION PERFORMANCE OF DNNE

	Overall wind power production	β (the first row WTs)	β (the second row WTs)	β (the third row WTs)	β (the fourth row WTs)
MAPE	4.37%	8.86%	9.70%	9.98%	13.62%
nRMSE	6.08%	10.05%	11.32%	11.39%	12.63%

2) Performance of the Proposed Control under Different Wind Prediction Intervals

As discussed in Section IV, the wind speed forecast data in the receding horizon is generated via the quantile-based Seq2Seq LSTM network. By examining the finite quantile levels τ from 2% and 98% to 15% and 85% (i.e. the PIs with 96% to 70% confidence levels) are yielded. A set of wind speed for 15 min is used to test the proposed control scheme. The prediction results under different PIs are given in Fig. 7. The corresponding total mileage payment and the dynamic performance of WTs are given in Table II and Fig. 8 (the weighting coefficient α is determined as 0.5). As indicated in Table II, compared with the conventional strategy that each WT operates at the MPPT mode, the total mileage payment is significantly reduced with the proposed control scheme regardless of the prediction confidence level. It can be found that the wind power is effectively smoothed out after introducing the proposed control, as shown in Fig. 8(a). Since a robust strategy is adopted to handle wind uncertainty, to prepare for the worst case, the total wind power production has a slight decrease along with the increase of the prediction confidence level (i.e. 10316.312895.38 kWh with 90%PI, 13192.65 kWh with 80%PI, 13405.88 kWh with 70%PI). To periodically trace the optimized dispatch commands, the rotor speed and pitch angle based control methods are simultaneous utilized in the proposed control. As shown in Fig. 8(b), (c), both the rotor speed and pitch angle of WTs in different rows vary within the allowable ranges $[\omega_{r\min}, \omega_{r\max}]$ and $[\beta_{\min}, \beta_{\max}]$. In particular, different from the conventional strategy that each WT operates at the MPPT mode, with the proposed control scheme, the pitch angle upstream WTs is not equal to zero, such that the spilled energy can be captured by downstream WTs, which increases the aggregated wind power production of when more power is expected. To sum up, the power regulation potential of the WF is optimally exploited with the proposed control scheme.

TABLE II
MILEAGE PAYMENT UNDER DIFFERENT WIND SPEED PIS

	96% PI	94% PI	92% PI	90% PI	80% PI	70% PI	Each WT with MPPT control
Total mileage payment ($)	407.73	411.40	415.44	417.69	424.13	431.00	630.54

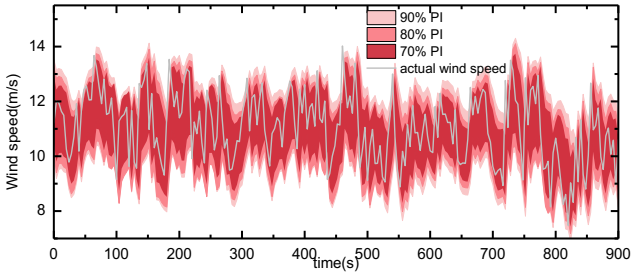

Fig. 7. Predicted wind speed with different PIs

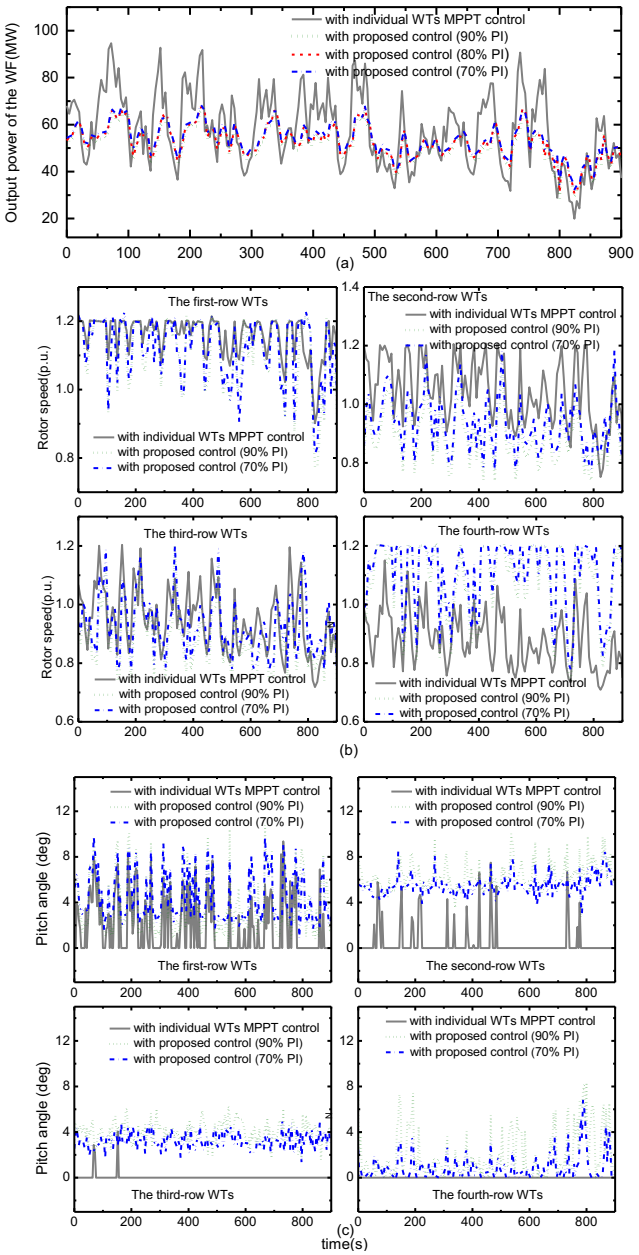

Fig. 8. Simulation results with different wind speed PIs. (a) total output power of WF, (b) rotor speed of WTs in different rows, (c) pitch angle of WTs in different rows

3) Performance of the Proposed Control under Different Weighting Factor

To investigate the influence of the adjustment of the weighting factor, scenarios with different α settings are investigated in this work. The simulation results in terms of α = 0.5 have given in Table II and Fig. 8. Under situations that α = 0.4, and α = 0.6, the total mileage payment of the dynamic operation status of WTs in different rows are given in Table III and Fig. 9. As indicated in table III, the mileage payment increases with the increase of α. This is because the increase of α means more attention is paid to wind power maximization, which in turn intensifies the total balancing cost. As shown in Fig. 9(a), the energy yield from the WF decreases with the decrease of α (i.e. the total captured energy throughout simulation is 14143.01kWh when α = 0.6 and 12301.21kWh when α = 0.4). According to Fig. 9(b), 9(c), the rotor speed and pitch angle of different rows WTs both vary to adjust wind power output. Specifically, the total amount of rotor speed and pitch angle variations increase with the decrease of α. This is because the wind power is expected to be smoother with a lower α. As a result, the downward/upward wind power regulation requirements become stricter. The total curtailed wind energy with the proposed control throughout simulation compared with MPPT control is given in Table IV. It can be found that curtailed wind energy is decreased with the increase of α, which is consistent with what we mentioned in Section IV. C.

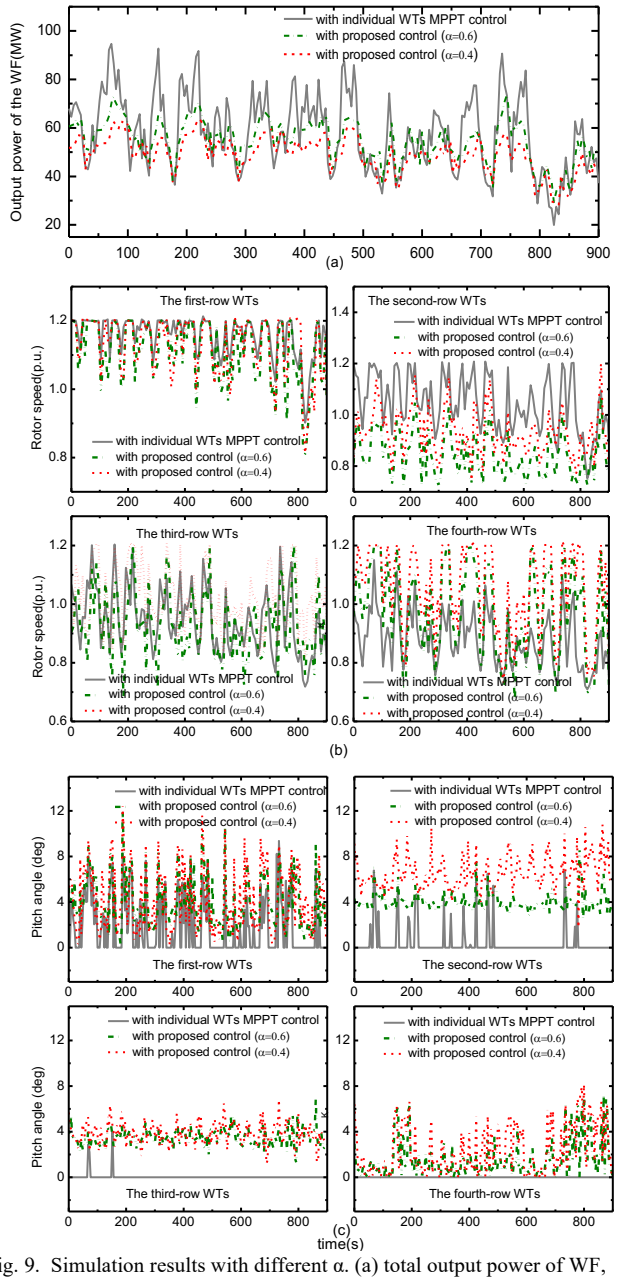

Fig. 9. Simulation results with different α. (a) total output power of WF, (b) rotor speed of WTs in different rows, (c) pitch angle of WTs in different rows

TABLE III
MILEAGE PAYMENT UNDER DIFFERENT α SETTINGS

	Total mileage payment ($)		Total mileage payment ($)

α =0.4, 96% PI	399.86	α =0.6, 96% PI	438.06
α =0.4, 94% PI	402.51	α =0.6, 94% PI	442.00
α =0.4, 92% PI	406.35	α =0.6, 92% PI	444.49
α =0.4, 90% PI	408.15	α =0.6, 90% PI	451.28
α =0.4, 80% PI	415.26	α =0.6, 80% PI	458.09
α =0.4, 70% PI	417.45	α =0.6, 70% PI	471.61

TABLE IV
TOTAL CURTAILED WIND ENERGY WITH PROPOSED CONTROL IN DIFFERENT SCENARIOS COMPARED WITH MPPT CONTROL

	Total curtailed wind energy (kWh)
α =0.5, 90% PI	1536.11
α =0.5, 80% PI	1238.84
α =0.5, 70% PI	1025.61
α =0.4, 90% PI	2130.28
α =0.6, 90% PI	849.99

VI. CONCLUSION

To mitigate the negative impact brought along by wind uncertainty and variability, this paper has proposed a novel wind power regulation scheme considering the resulting balancing cost. In particular, the internal wake effect in the WF has been taken into account. Besides, the wind uncertainty is well handled through a robust control method. To bypasses the time-consuming computation process caused by the high nonlinearity and non-convexity of the formulated optimization problem, a RVFL-based DNNE algorithm has been introduced. Simulations results have verified that the proposed control scheme can effectively manage the total power production of the WF via exploiting WTs' self-regulation capabilities. The obtained results indicate that the proposed control is a feasible solution to mitigate the power balancing dilemmas that brought along by high penetration of wind integration.

REFERENCES

[1] Q. Zhou, M. Shahidehpour, A. Paaso, S. Bahramirad, A. Alabdulwahab, and A. Abusorrah, "Distributed control and communication strategies in networked microgrids," *IEEE Communications Surveys & Tutorials,* vol. 22, pp. 2586-2633, 2020.

[2] J. M. Morales, A. J. Conejo, H. Madsen, P. Pinson, and M. Zugno, *Integrating renewables in electricity markets: operational problems* vol. 205: Springer Science & Business Media, 2013.

[3] *Balancing Responsibility and Costs of Wind Power Plants*. Available: http://www.ewea.org/fileadmin/files/library/publications/position-papers/EWEA-position-paper-balancing-responsibility-and-costs.pdf

[4] Bonneville Power Administration: Customer supplied wind balancing services pilot program, version 2. Retrieved February 2012, from Bonneville Power Administration (2011).http://transmission.bpa.gov/ts_business_practices/Content/PDF_files/Individual_BPs/Customer_Supplied_Wind_Balancing_Pilot.pdf

[5] "Tariff for maintaining and restoring the individual balance of access responsible parties," [Online]. Available: http://www.elia.be/~/media/files/Elia/Products-and services/Balancing/Imbalance_2012-2015_EN.pdf

[6] P. Cambron, R. Lepvrier, C. Masson, A. Tahan, and F. Pelletier, "Power curve monitoring using weighted moving average control charts," *Renewable Energy,* vol. 94, pp. 126-135, 2016.

[7] Q. Jiang and H. Wang, "Two-time-scale coordination control for a battery energy storage system to mitigate wind power fluctuations," *IEEE Transactions on Energy Conversion,* vol. 28, pp. 52-61, 2013.

[8] M. Khalid and A. Savkin, "Minimization and control of battery energy storage for wind power smoothing: Aggregated, distributed and semi-distributed storage," *Renewable Energy,* vol. 64, pp. 105-112, 2014.

[9] Y. Zhou, Z. Yan, and N. Li, "A novel state of charge feedback strategy in wind power smoothing based on short-term forecast and scenario analysis," *IEEE Transactions on Sustainable Energy,* vol. 8, pp. 870-879, 2017.

[10] X. Lyu, Y. Jia, Z. Xu, and J. Ostergaard, "Mileage-responsive Wind Power Smoothing," *IEEE Transactions on Industrial Electronics,* 2019.

[11] V. Nelson, *Wind energy: renewable energy and the environment*: CRC press, 2013.

[12] J. R. Abbad, "Electricity market participation of wind farms: the success story of the Spanish pragmatism," *Energy policy,* vol. 38, pp. 3174-3179, 2010.

[13] A. Hellmers, M. Zugno, A. Skajaa, and J. M. Morales, "Operational strategies for a portfolio of wind farms and CHP plants in a two-price balancing market," *IEEE Transactions on Power Systems,* vol. 31, pp. 2182-2191, 2015.

[14] R. Zhang, T. Jiang, F. F. Li, G. Li, H. Chen, and X. Li, "Coordinated bidding strategy of wind farms and power-to-gas facilities using a cooperative game approach," *IEEE Transactions on Sustainable Energy,* 2020.

[15] Z. Wu, M. Zhou, J. Wang, E. Du, N. Zhang, and G. Li, "Profit-sharing mechanism for aggregation of wind farms and concentrating solar power," *IEEE Transactions on Sustainable Energy,* 2020.

[16] E. Du, N. Zhang, C. Kang, B. Kroposki, H. Huang, M. Miao*, et al.*, "Managing wind power uncertainty through strategic reserve purchasing," *IEEE Transactions on Power Systems,* vol. 32, pp. 2547-2559, 2016.

[17] Q. Zhou, Z. Tian, M. Shahidehpour, X. Liu, A. Alabdulwahab, and A. Abusorrah, "Optimal consensus-based distributed control strategy for coordinated operation of networked microgrids," *IEEE Transactions on Power Systems,* vol. 35, pp. 2452-2462, 2019.

[18] J.-A. Dahlberg, "Assessment of the lillgrund wind farm: power performance wake effects," *Vattenfall Vindkraft AB, 6_1 LG Pilot Report, http://www. vattenfall. se/sv/file/15_Assessment_of_the_Lillgrund_W. pdf_16596737. pdf (cited March 30, 2012),* 2009.

[19] J. S. González, M. B. Payán, J. R. Santos, and Á. G. G. Rodríguez, "Maximizing the overall production of wind farms by setting the individual operating point of wind turbines," *Renewable Energy,* vol. 80, pp. 219-229, 2015.

[20] N. Gionfra, G. Sandou, H. Siguerdidjane, D. Faille, and P. Loevenbruck, "Wind farm distributed PSO-based control for constrained power generation maximization," *Renewable Energy,* 2018.

[21] J. Park and K. H. Law, "A data-driven, cooperative wind farm control to maximize the total power production," *Applied Energy,* vol. 165, pp. 151-165, 2016.

[22] J. R. Marden, S. D. Ruben, and L. Y. Pao, "A model-free approach to wind farm control using game theoretic methods," *IEEE Transactions on Control Systems Technology,* vol. 21, pp. 1207-1214, 2013.

[23] A. S. Ahmadyar and G. Verbič, "Coordinated operation strategy of wind farms for frequency control by exploring wake interaction," *IEEE Transactions on Sustainable Energy,* vol. 8, pp. 230-238, 2017.

[24] X. Lyu, Y. Jia, and Z. Xu, "A novel control strategy for wind farm active power regulation considering wake interaction," *IEEE Transactions on Sustainable Energy,* vol. 11, pp. 618-628, 2019.

[25] N. A. Janssens, G. Lambin, and N. Bragard, "Active power control strategies of DFIG wind turbines," in *2007 IEEE Lausanne Power Tech*, Lausanne, Switzerland, 2007, pp. 516-521.

[26] N. R. Ullah, K. Bhattacharya, and T. Thiringer, "Wind farms as reactive power ancillary service providers—technical and economic issues," *IEEE Transactions on Energy Conversion,* vol. 24, pp. 661-672, 2009.

[27] S. Wang and K. Tomsovic, "A novel active power control framework for wind turbine generators to improve frequency response," *IEEE Transactions on Power Systems,* vol. 33, pp. 6579-6589, 2018.

[28] S. Hochreiter and J. Schmidhuber, "Long short-term memory," *Neural computation,* vol. 9, pp. 1735-1780, 1997.

[29] I. Steinwart and A. Christmann, "Estimating conditional quantiles with the help of the pinball loss," *Bernoulli,* vol. 17, pp. 211-225, 2011.

[30] Y. Jia, Z. Xu, L. L. Lai, and K. P. Wong, "Risk-based power system security analysis considering cascading outages," *IEEE Transactions on Industrial Informatics,* vol. 12, pp. 872-882, 2015.

[31] J. Jonkman, S. Butterfield, W. Musial, and G. Scott, "Definition of a 5-MW reference wind turbine for offshore system development," National Renewable Energy Lab.(NREL), Golden, CO (United States)2009.

[32] *Dynamic IEEE Test Systems*. Available: https://www2.kios.ucy.ac.cy/testsystems/index.php/ieee-9-bus-modified-test-system/

[33] *UCAR/NCAR - Earth Observing Laboratory. 2013. PCAPS ISFS 1 second data. Version 1.0. UCAR/NCAR - Earth Observing Laboratory*. Available: https://data.eol.ucar.edu/dataset/233.003

Xue Lyu (S'16, M'19) received her B.Eng. degree from Qingdao University of Technology, China, in 2013; M. Eng. degree from Shanghai University of Electric Power, China, in 2016, and Ph.D. degree from The Hong Kong Polytechnic University, Hong Kong, in 2019. She is now a postdoctoral fellow at the University of Hong Kong. She is also a visiting scholar in the Department of Electrical and Electronic Engineering, Southern University of Science and Technology, Shenzhen, China. Her research interests include control and optimization for grid-integration of renewable energy systems.

Youwei Jia (S'11, M'15) received the B.Eng and Ph.D degrees from Sichuan University, China, in 2011, and The Hong Kong Polytechnic University, Hong Kong, in 2015, respectively. From 2015 to 2018, he was a postdoctoral fellow at The Hong Kong Polytechnic University. He is currently an Assistant Professor with the Department of Electrical and Electronic Engineering, University Key Laboratory of Advanced Wireless Communication of Guangdong Province and Shenzhen Key Laboratory of Electrical Direct Drive Technology, Southern University of Science and Technology, Shenzhen, China. His research interests include microgrid, renewable energy modeling and control, power system security analysis, complex network and artificial intelligence in power engineering.

Tao Liu (M'13) received his BE degree from Northeastern University, China, in 2003 and PhD degree from the Australian National University (ANU), Australia, in 2011. From 2012 to 2015, he worked as a Post-doctoral Fellow at ANU, University of Groningen, and University of Hong Kong (HKU). He became a Research Assistant Professor at HKU in 2015 and now is an Assistant Professor. His research interests include power system analysis and control, complex dynamical networks, distributed control, and event-triggered control.

Songjian Chai (M'18) received his M.S. and Ph.D. degrees in electrical engineering from the Hong Kong Polytechnic University, Hong Kong, in 2012 and 2018, respectively. He is currently a Postdoctoral Research Fellow in Shenzhen University, Shenzhen, China. His research interests include variable renewable generation forecasting, electricity price forecasting, power system uncertainty analysis and artificial intelligence application in power engineering.